Macromolecules



pubs.acs.org/Macromolecules
Article

# Hydration Dynamics of Perdeuterated PNIPAM in Aqueous Solution

Christine M. Papadakis,* Eric Rende, Feifei Zheng, Bahar Yazdanshenas, Marcell Wolf, Michaela Zamponi, Marie-Sousai Appavou, Thomas Müller, Dharani Mullapudi, Alec Nieth, Dirk Schanzenbach, André Laschewsky, and Alfons Schulte*

Cite This: *Macromolecules* 2026, 59, 4124–4133



**ABSTRACT:** Perdeuterated poly(*N*-isopropylacrylamide) (PNIPAM-d10) is synthesized by free radical polymerization and characterized by $^2$H NMR, Fourier-transform infrared, and Raman spectroscopy. A concentrated solution of this polymer in $H_2O$ is investigated with respect to the dynamics of the hydration and bulk water using quasi-elastic neutron scattering. Due to the exchange of the protons in the polymer with deuterons, the incoherent neutron scattering from the polymer is suppressed, offsetting apart the hydration water. Deuteration causes a remarkable upward shift of the cloud point temperature by 4 °C. It is found that, when heating through the cloud point, the fraction of hydration water decreases abruptly. The relaxation time of the hydration water is consistently lower than the one observed previously for PNIPAM in $H_2O$. Raman spectroscopy of the CD bands across the demixing transition shows a frequency shift consistent with polymer dehydration.

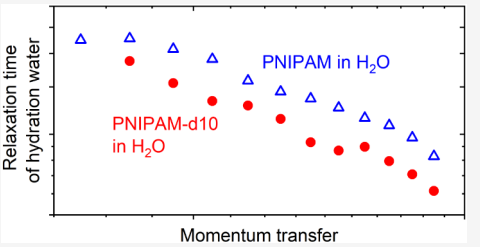




## 1. INTRODUCTION

The interaction of water with biological and man-made macromolecules plays a key role in their structural, dynamic, and functional properties.[1,2] The hydrogen bond network and hydration shell are crucial for the function and stability of biomolecules. In particular, the hydrophobic effect stabilizes native protein structures at ambient conditions.[3,4] Synthetic nonionic thermoresponsive polymers typically feature simple repeating units consisting of hydrophobic and polar groups with comparable water interactions. The thermoresponsive polymers of lower critical solution temperature (LCST) type are water-soluble at low temperatures but become water-insoluble above the cloud point temperature, $T_{cp}$, where they dehydrate, which induces a chain collapse, provided the backbone is sufficiently flexible.[5] Thus, a demixing transition takes place when they are heated through the cloud point temperature, $T_{cp}$.[6,7] This transition is closely associated with aggregate formation and a reduction in the amount of hydration water.[8]

In numerous studies, particularly those using small-angle neutron scattering, heavy water ($D_2O$) was used in place of $H_2O$ to reduce the incoherent background of the solvent. In proton nuclear magnetic resonance, using $D_2O$ instead of $H_2O$ reduces the overlap of polymer and water signals.[9−11] For aqueous solutions of LCST-type thermoresponsive polymers and microgels, replacing $H_2O$ by $D_2O$ typically, merely results in a small shift of $T_{cp}$, but not in a qualitative change in behavior.[6,12] This shift may be attributed to the different properties of $D_2O$ compared to those of $H_2O$ because nuclear quantum effects alter the strength of various types of hydrogen bonds.[13] $H_2O$ and $D_2O$ have different melting points, specific heat capacities, viscosities, and acidities, and they differ in their local packing.[13] Thus, exchanging $H_2O$ by $D_2O$ in a polymer solution is not only advantageous from the experimental point of view but may also be exploited to deepen the understanding of the interactions between the polymer and water, e.g., regarding the hydrogen bonds between the polymer and water or the formation of a structured water cage around hydrophobic groups of the polymer.[14] For aqueous solvents, it was found recently that the hydrogen bond dynamics in $D_2O$ is ca. 25% slower than in $H_2O$.[15]

Exchanging the hydrogen atoms with deuterium in a polymer provides valuable insights in changes in chemical bonding and band assignments through vibrational spectroscopy, as isotope editing causes characteristic frequency shifts. In the past, deuteration of polymers was also used to enhance the scattering contrast in neutron scattering, e.g., in blends of deuterated and protiated polymers to determine the domain sizes (seminal work was carried out by Higgins, as reviewed in ref 16), or in melts of block copolymers having one deuterated block to determine the morphologies and repeat distances[17] as well as their conformation,[18] or in polymers with side chains for the determination of the local order by means of the partial structure factors.[19] However, such studies have often been limited by the availability of deuterated monomers needed for the synthesis of such polymers. There has been recent progress

Received: November 19, 2025
Revised: March 6, 2026
Accepted: March 11, 2026
Published: March 19, 2026





https://doi.org/10.1021/acs.macromol.5c03241
*Macromolecules* 2026, 59, 4124−4133

in the synthesis and availability of synthetic deuterated monomers and polymers, opening new avenues to characterize the effects of polymer deuteration in model systems.

Here, we present an investigation of a perdeuterated thermoresponsive polymer, namely, poly(*N*-isopropylacrylamide) (PNIPAM-d10), in $H_2O$. Our study relates the macroscopic phase behavior with the hydration dynamics across the cloud point. The protiated analog, PNIPAM, in aqueous solution, is a well-studied system, both in $H_2O$ and $D_2O$,[20] and only minor changes have been observed regarding the phase behavior in both solvents.[21] In $H_2O$, its cloud point is at ca. 32 °C, which is rather independent of molar mass and concentration over a wide range.[20] Above $T_{cp}$, the polymers become water-insoluble, the solvated polymer coils collapse, and form long-lived mesoscopic aggregates named "mesoglobules".[22−28] The arrest of their growth is due to their low water content, which, due to the resulting low polymer mobility, hampers macroscopic phase separation.[29]

Our previous investigations on a concentrated (25 wt %) solution of PNIPAM in $D_2O$ using Raman spectroscopy revealed that the hydrophobic isopropyl groups in the side chains are dehydrated at $T_{cp}$.[29] At atmospheric pressure, this dehydration proceeds abruptly, i.e., within 2 °C.[29] These experimental findings on a concentrated solution were confirmed by atomistic computer simulations on a single chain.[30]

Quasi-elastic neutron scattering (QENS) is the method of choice to characterize the water in aqueous solutions of thermoresponsive polymers, namely the fractions of hydration water and bulk water, and to characterize their dynamics.[31] In our previous studies on a 25 wt % PNIPAM solution in $H_2O$,[32,33] the hydration water was characterized by measuring the dynamic structure factor $S(q, \Delta E)$ ($q$ is the momentum transfer and $\Delta E$ the energy transfer) in wide ranges of $q$ and $\Delta E$. By transforming $S(q, \Delta E)$ into the imaginary part of the dynamic susceptibility $\chi''(q, \nu)$, where $\nu$ is the frequency, the contribution from hydration water could be clearly distinguished from the ones of bulk water.[33] It was revealed that the fraction of hydration water decreases abruptly at the cloud point (from 0.28 to 0.17 between 35.5 and 37.4 °C). From the $q$-dependence of the relaxation time of the hydration water, it was found that it follows a jump diffusion process.[33] The elastic line strength decreases abruptly, i.e., the mean-square displacement of $H_2O$ and the PNIPAM segments decreases abruptly, which reflects the chain collapse.[33] While these results gave unprecedented information about the behavior of the hydration water, there is still a contribution to the susceptibility from incoherent scattering by the polymer. For the system under study, it was estimated that a fraction as large as 22% of the neutrons were scattered by PNIPAM (and not by $H_2O$). In the present study, we employ perdeuterated PNIPAM-d10 to minimize the polymer signal in QENS. In this polymer, all carbon−hydrogen bonds are deuterated; i.e., 10 out of the 11 hydrogen atoms are replaced by deuterium, which reduces the fraction of neutrons scattered by the polymer to ca. 3%. Only the slightly acidic nitrogen-bound hydrogen of the amide moiety is not deuterated, as it is subject to H-D exchange with $H_2O$.[34] In addition, deuteration provides a new avenue to study polymer−water interactions.

When comparing the results from thermoresponsive protiated polymers and their deuterated versions, one should keep in mind, though, that not only do the scattering cross sections change, but also the interactions of the repeating units with water are affected. For instance, the onset temperature of the coil-to-globule transition, as determined by differential scanning calorimetry, was found at 31 °C for dispersions of microgels from PNIPAM in $H_2O$, whereas it was shifted to 34−35 °C for microgels from PNIPAM-d10 in $H_2O$ (range of polymer concentrations: 10−40 wt %).[12] This shift was tentatively attributed to the less favorable contacts between the hydrophobic groups in the polymers with each other for PNIPAM-d10 than in PNIPAM. An upward shift of the volume phase transition temperature (VPTT) was also observed in dispersions of microgels from perdeuterated *N*-isopropyl methacrylamide, NIPMAM-d12, in $H_2O$ compared to the fully hydrogenated NIPMAM microgels.[35] It was attributed to the increase in the basicity of the isopropyl group by deuteration, an alteration of the hydrogen bonding network, and the fact that, in the NIPMAM-d12 system, polymer−polymer and solvent−solvent interactions are less favorable than solvent−polymer interactions.

Studies on aqueous dispersions of microgels from partially deuterated repeating units, e.g., NIPAM-d7 (isopropyl group in the side group deuterated)[36−38] or NIPAM-d3 (vinyl group in the backbone deuterated),[39] gave further insights. For the VPTT of NIPAM-d7 microgels in $H_2O$, an upward shift of a few degrees centigrade was found compared to microgels from protiated NIPAM.[36,37] In contrast, in dispersions of NIPAM-d3 microgels in $H_2O$, this shift was virtually absent[37] or amounted to only 1−2 °C.[39] Hence, the hydrophobic isopropyl group seems to be at the origin of the shift of VPTT rather than the backbone vinyl group. The shift of the VPTT by deuteration was explained by different Flory−Huggins parameters between the respective repeating unit and the solvent.[38] To the best of our knowledge, no experimental studies of the molecular interactions between the deuterated thermoresponsive polymers and water have been carried out.

Here, we investigate the water dynamics of a 25 wt % solution of a PNIPAM-d10 homopolymer in $H_2O$ across the LCST transition. We present the synthesis and molecular characterization of the polymer. Optical microscopy (OM) reveals the cloud point temperature, $T_{cp}$. Raman spectroscopy is used to analyze the vibrational dynamics of the perdeuterated alkyl groups and their changes at $T_{cp}$. QENS provides a thorough investigation of the dynamics of bulk and hydration water over a wide temperature range across $T_{cp}$. We find that $T_{cp}$ is significantly shifted upward, namely by 4 °C compared to that of protiated PNIPAM in $H_2O$, and that the relaxation time of the hydration water is consistently lower.

## 2. MATERIALS AND METHODS

### 2.1. Materials

**2.1.1. Purification of *N*-isopropyl-d7 Acrylamide-d3 (NIPAM-d10).** 2.00 g of NIPAM-d10 ($C_6HD_{10}NO$, Polymer Source, Inc., Lot-# P41237) in 7.5 mL of *n*-heptane (Merck UVASOL, spectroscopic grade) and 0.75 mL of freshly distilled, thiophene-free benzene were heated to a slight reflux. The resulting light yellow, almost clear solution was slowly cooled to room temperature and then cooled further in a refrigerator to 3 °C to make the monomer precipitate. After standing overnight at this temperature, the still yellowish precipitate was filtered off via a glass filter frit (por. G3) and washed twice with cold *n*-heptane. Crystallization was repeated under the same conditions to yield 1.91 g of an almost colorless, fine powder after filtration and drying under vacuum. The protiated analog *N*-isopropyl-acrylamide (NIPAM, $C_6H_{11}NO$, TCI, Lot-# 8RMDN) was purified in the same way, yielding colorless needles.



https://doi.org/10.1021/acs.macromol.5c03241
Macromolecules 2026, 59, 4124−4133

**2.1.2. Polymerization.** An argon-flushed 50 mL round-bottom flask with a silicone septum, gas inlet, and magnetic stirrer was charged with 1.80 g (14.61 mmol) of crystallized NIPAM-d10, 12.0 mg (73 $\mu$mol, 0.5 mol % relative to monomer) of 2,2′-azobis(2-methylpropionitrile) (AIBN, freshly recrystallized from methanol), and 9.5 mL of tetrahydrofuran (THF, freshly distilled from potassium/benzophenone). After complete dissolution of the solid reactants, the mixture was cooled by an ice−water bath, and a slow stream of argon gas was bubbled through the solution for 30 min. Then, the mixture was stirred at 60 °C for 18 h under an argon atmosphere. The reaction was stopped by cooling the yellowish, almost solid reaction mixture to room temperature and allowing air to enter the flask. For work-up, another 6 mL of THF was added, and stirring was continued to dissolve the crude product. The polymer was precipitated by using a vigorously stirred mixture of 300 mL of hexane and 200 mL of diethyl ether. The precipitate was filtered off, dried *in vacuo*, and dissolved in 12 mL of THF to repeat the precipitation under the same conditions. The precipitate was filtered off, vacuum-dried, dissolved in 150 mL of deionized water, and freeze-dried to yield 1.74 g of a fluffy, hygroscopic, colorless powder.

**2.1.3. Analytical Data.** $^2$H NMR (92 MHz, Bruker Avance III 600 spectrometer) in acetone, $\delta$ [ppm]: 1.14 ($CD_3$), 0.8∼2.6 (very broad signal, $CD_2$ and CD of the main chain), 3.8∼4.4 (broad signal, C−D of the isopropyl group).

FT-IR (KBr pellet), $\nu$ [cm$^{-1}$]: 3438, 3306, 3066, 2941, 2229, 2158, 2068, 1646, 1542, 1317, 1188, 1056, 630 (selected bands).

Size exclusion chromatography (SEC), eluent *N*-methylpyrrolidone (NMP) with 0.5 wt % of LiBr: monomodal distribution, apparent weight-average molar mass $M_w^{app}$ = 22850 g·mol$^{-1}$, dispersity Đ = 2.7 (calibration by narrowly distributed polystyrene standards. Precolumn PSS GRAM 10 $\mu$m, 8 × 50 mm, main column PSS GRAM Linear 7 $\mu$m, 8 × 300 mm. 0.500 mL·min$^{-1}$, detector: Shimadzu RID-6A).

Thermogravimetric analysis (TGA, under nitrogen, heating rate 10 K·min$^{-1}$): onset of decomposition at $T_{dec}^{onset} \cong$ 250 °C. Differential scanning calorimetry (DSC, heating rate 10 K·min$^{-1}$): glass transition temperature $T_g$ at 132 °C.

A protiated PNIPAm reference was prepared in the same way, yielding quantitatively the polymer as a fluffy, hygroscopic, colorless powder. FT-IR (KBr pellet), $\nu$ [cm$^{-1}$]: 3436, 3306, 3075, 2973, 2935, 2876, 1650, 1544, 1461, 1387, 1368, 1174, 1131, 625 (selected bands). Apparent weight-average molar mass by SEC: $M_w^{app}$ = 25540 g·mol$^{-1}$, dispersity Đ = 2.3 (calibration by narrowly distributed polystyrene standards), onset of decomposition at $T_{dec}^{onset} \cong$ 250 °C (TGA, under nitrogen, heating rate 10 K·min$^{-1}$), glass transition temperature $T_g$ at 127 °C (DSC, heating rate 10 K·min$^{-1}$).

**2.1.4. Sample Preparation.** For optical microscopy (OM), Raman spectroscopy, neutron diffraction, and QENS experiments, PNIPAM-d10 was dissolved in deionized $H_2O$ at polymer concentrations of 24.5−26.7 wt %. The coherent and incoherent neutron scattering cross sections are listed in Table 1. From the molar ratio of the NIPAM-d10 repeating unit and $H_2O$ of 1:19, it is estimated that ca. 97% of the incoherently scattered neutrons stem from $H_2O$ (and only ca. 3% from PNIPAM-d10).

**Table 1. Calculated Incoherent and Coherent Neutron Scattering Cross Sections for NIPAM-d10 Repeating Units and $H_2O$**

| Component | Incoherent cross section (barn) | Coherent cross section (barn) |
|---|---|---|
| NIPAM-d10 | 101.28 | 106.23 |
| $H_2O$ | 160.54 | 7.74 |

## 2.2. Methods

**2.2.1. Raman Spectroscopy and Optical Microscopy.** Raman spectroscopy was performed using a LabRam HR 800 system (JY Horiba), employing excitation from a Helium-Neon laser with a wavelength of 633 nm (for details, see ref 29). The sample solution was contained in a sealed microcapillary with an outer diameter of 350 $\mu$m. The capillary was anchored in a copper block that was attached to a circulating bath thermostat. The sample temperature was measured with a Pt-100 resistance thermometer inside the copper block. The temperature was corrected for radiation losses due to the microscope objective, as described in ref 29. Temperature-dependent measurements were carried out in the C−D stretch region with a spectral resolution of 2 cm$^{-1}$. The laser power at the sample position was less than 3 mW at a spot size of 1.5 $\mu$m. Following each temperature change, the sample was equilibrated for 10 min, and the spectra were acquired with an integration time of 200 s. The raw data were analyzed by using OriginLab software to determine peak frequency positions after smoothing and background subtraction. Optical microscopy was carried out in the same microcapillary cell as that used for Raman spectroscopy. Images were acquired with a CCD camera on the port of an Olympus X41 microscope.

**2.2.2. Neutron Diffraction Measurements with Polarization Analysis.** These were performed at the DNS instrument of JCNS at the Heinz Maier-Leibnitz-Zentrum (MLZ), Garching, Germany.[19,40] With an incident wavelength of 4.74 Å and an angular scattering range from 5° to 125°, the $q$-range from 0.12 to 2.3 Å$^{-1}$ was covered. The solution was mounted in a cylindrical Al cell with a 0.5 mm gap. The sample was investigated at selected temperatures between 21 and 52 °C. The background was measured on an empty cell and subtracted by applying the corresponding transmission-dependent corrections.

**2.2.3. Quasi-Elastic Neutron Scattering (QENS).** These experiments were carried out at the time-of-flight spectrometer TOFTOF at MLZ.[41,42] Measurements were conducted in a similar way as in our previous experiment.[33] In brief, a wavelength of the incident neutron beam of 6 Å, along with a rotation speed of the chopper system of 16000 rpm, was selected. The sample was mounted in an aluminum (EN AW-7075) pressure cell, similar to the one used previously,[43] but with only 6 channels having a diameter of 0.6 mm each. This way, only 0.5 mL of sample was needed. (A pressure cell was used for possible high-pressure experiments.) The cell was placed at an angle of 135° with respect to the incident neutron beam. A heating scan was performed on the PNIPAM-d10 solution in $H_2O$ from 25 to 52 °C in steps of 2−5 °C. The measuring time at each temperature was 60 min, with a 30-min equilibration time after each temperature change. Reversibility was verified after cooling and waiting for thermal equilibration for 1 h. The accessible range of momentum transfers, $q$, was 0.15 to 1.85 Å$^{-1}$. The spectra were normalized to the incoming neutron flux and a vanadium standard measurement. The signal from an empty cell measurement (duration of 2 h) was subtracted from the data. At this, the $q$-dependent self-shielding correction was carried out following the Paalman−Pings procedure.[44,45] A thin vanadium slab was measured for 2 h to perform background corrections and calibrations. These operations were performed using the TOFTOF data reduction routines within Mantid,[46] giving the dynamic structure factor $S(q, \Delta E)$, where $\Delta E$ is the energy transfer. The $S(q, \Delta E)$ data were converted into the imaginary part of the dynamic susceptibility, $\chi(q, \nu)$, where $\nu = \Delta E/h$ ($h$ is Planck's constant), using a self-written code in Python.[33] For simplicity, we refer to it here as $\chi(q, \nu)$. The transformation was carried out as follows:[47,48]

$$\chi(q, \nu) \propto \frac{S(q, -\nu)}{n_B(\nu)} \tag{1}$$

with the Bose factor

$$n_B(\nu) = \left[\exp\left(\frac{h\nu}{k_B T}\right) - 1\right]^{-1} \tag{2}$$

where $k_B$ is the Boltzmann constant and $T$ the absolute temperature. The dynamic susceptibilities were fitted by means of the following expressions:

(i) The Debye function for the diffusional (d) and the effective local (l) process of bulk water:



https://doi.org/10.1021/acs.macromol.5c03241
Macromolecules 2026, 59, 4124−4133

$$\chi_j(q,\nu) = -\mathrm{Im}\left(\frac{C_j(q)}{1 + 2\pi i\tau_j\nu}\right) \quad (3)$$

where $C_j(q)$ is a $q$-dependent scaling factor. The index $j$ stands for d or l. $\tau_j$ denotes the relaxation time, which is related to the peak frequency $\nu_{max,j}$ by $\tau_j = (2\pi\nu_{max,j})^{-1}$.

(ii) The damped harmonic oscillator (DHO) for the vibrational process:

$$\chi_v(q,\nu) = -\mathrm{Im}\left(\frac{C_v(q)\nu_0^2}{\nu^2 - \nu_0^2 - (i\nu\Gamma/2\pi)}\right) \quad (4)$$

with $C_v(q)$ as a scaling factor, $\nu_{max,v}$ as the peak frequency, and $\Gamma$ as the width at half-maximum.

(iii) The Cole-Davidson function with an exponent of 0.7 for the hydration water:

$$\chi_h(q,\nu) = -\mathrm{Im}\left(\frac{C_h(q)}{(1 + 2\pi i\tau_h\nu)^{0.7}}\right) \quad (5)$$

with $C_h(q)$ as a scaling constant and $\tau_h$ as the relaxation time.

(iv) The elastic line was modeled using the resolution function measured with a vanadium standard, $\chi_{res}(q,\nu)$, multiplied by a scaling factor of $C_{el}(q)$:

$$\chi_{el}(q,\nu) = C_{el}(q)\chi_{res}(q,\nu) \quad (6)$$

The elastic line comprises very slow processes, beyond the resolution limit of the experiment.

**2.2.4. High-Resolution QENS.** These experiments were carried out on the same sample at the backscattering spectrometer SPHERES at MLZ.[49,50] A range of energy transfers between −0.03 and 0.03 meV was covered with a resolution of 0.65 $\mu$eV (fwhm) as well as a $q$-range of 0.22−1.8 Å$^{-1}$. The solution was mounted in a cylindrical Al cell with a 0.1 mm gap. Measurement times were 8 h. After each temperature change, the sample was allowed to equilibrate thermally for 30 min. The sample environment was filled with He gas of ca. 100 mbar to suppress evaporation of $H_2O$ from the sample. The background from the empty cell was measured for about 6 h and was subtracted from the solution spectra. The resolution of the instrument was measured by using the sample that had been cooled to 3 K. The detector efficiency was determined by measuring a cylindrical vanadium sample having a thickness of 1 mm for 30 min.

## 3. RESULTS AND DISCUSSION

### 3.1. Synthesis and Molecular Characterization

The perdeuterated polymer PNIPAM-d10 was synthesized by free radical solution polymerization in THF. The moderate molar mass achieved ($M_w^{app}$ = 23 kg·mol$^{-1}$) and the relatively high dispersity (Đ ≅ 2.7) after workup are explained by the high monomer conversion (>95%). The comparison of the $^2$H NMR spectra of the monomer and the polymer (both in acetone, Figure 1) demonstrates the absence of monomer in the product. Otherwise, the shapes of the spectra correspond qualitatively to the ones of their protiated counterparts[51] except for the massive broadening of the methine and methylene signals of the polymer backbone. Also, the thermo-analytical data of the perdeuterated PNIPAM-d10 (onset of decomposition at $T_{dec}^{onset}$ ≅ 250 °C, glass transition temperature $T_g$ = 132 °C) correspond closely to the ones of the protiated analogue.[52]

In contrast, the IR spectrum of PNIPAM-d10 (Figure 2) shows characteristic differences with respect to its protiated counterpart, as the vibration frequencies of the H- and D-related bands differ strongly. For instance, the characteristic CH stretching bands of protiated PNIPAM[53−55] at about 2970, 2935, and 2875 cm$^{-1}$ and the bending signals at about

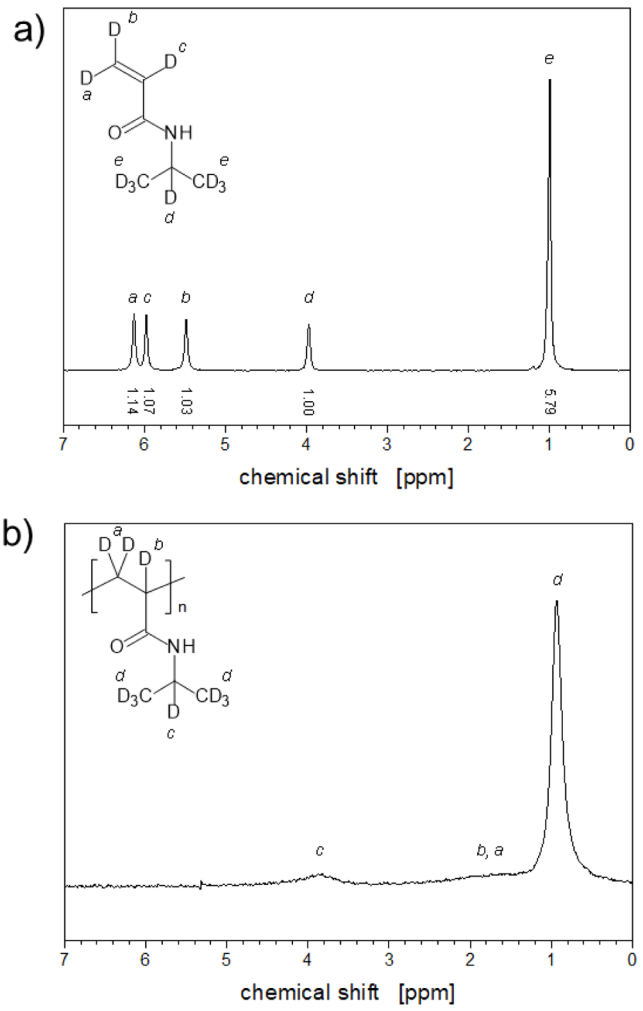


**Figure 1.** $^2$H NMR spectra of (a) perdeuterated monomer NIPAM-d10 and (b) polymer PNIPAM-d10 in acetone.

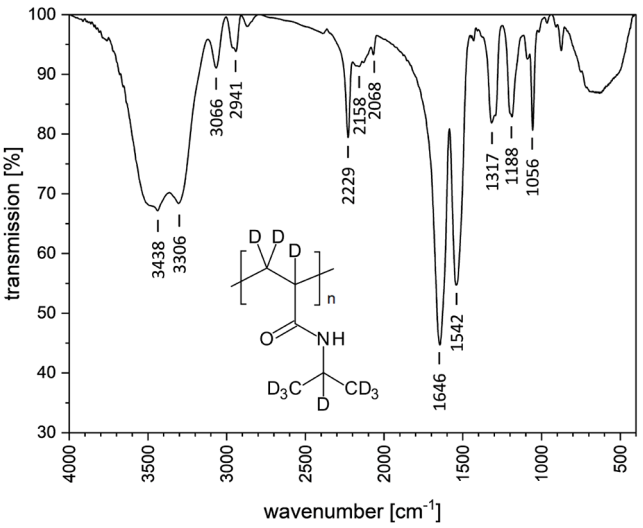


**Figure 2.** Transmission FTIR spectrum of perdeuterated polymer PNIPAM-d10 (KBr pellet).

1460 and 1380 cm$^{-1}$ are missing. Instead, new bands are visible for PNIPAM-d10 in the range from 2250 to 2050 cm$^{-1}$ that are characteristic of the CD stretching bands. The amide I and II bands, however, at about 1645 and 1540 cm$^{-1}$ as well as


https://doi.org/10.1021/acs.macromol.5c03241
Macromolecules 2026, 59, 4124−4133

the NH-stretching band at about 3310 $cm^{-1}$, are present for both PNIPAM and PNIPAM-d10, in agreement with the expectations.

Raman spectra of PNIPAM-d10 and the analogous PNIPAM are shown in Figure 3 over the frequency range of

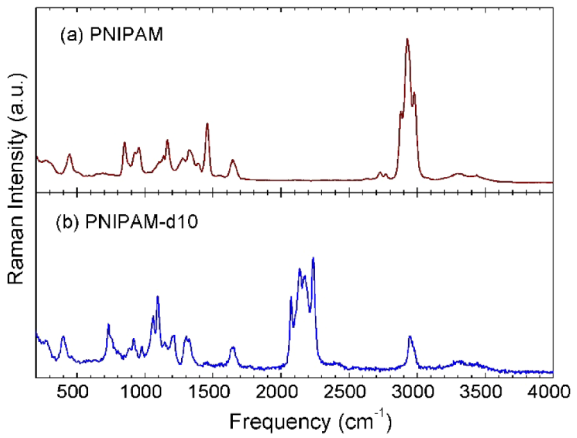


**Figure 3.** Raman spectra of PNIPAM (a) and PNIPAM-d10 (b).

200 to 4000 $cm^{-1}$. We can distinguish the following main spectral bands: The bands assigned to C−H deformation modes are observable between 1350 and 1450 $cm^{-1}$. The vibrational bands due to C−H groups are discernible in the ranges 2850 and 3000 $cm^{-1}$ while the bands between 1500 and 1750 $cm^{-1}$ are assigned to the amide vibrations. Upon deuteration, the C−H stretch vibrational bands shift to lower wavenumbers (2000−2350 $cm^{-1}$ range) due to the isotope effect. Four subbands are clearly resolved. There are also shifts in the amide and C−D deformation modes.

### 3.2. Demixing Transition

The demixing transition was characterized by using optical microscopy. Figure S1 in the Supporting Information (SI) shows images at temperatures of 34 and 37 °C. From the darkening in these images, we estimate that $T_{cp}$ is 36 ± 2 °C. This value is in good agreement with the temperature-dependent frequency shift of the C−D stretch bands[56] and is consistent with the QENS data (see below). Remarkably, $T_{cp}$ is 4 °C higher than that of protiated PNIPAM.

### 3.3. Hydration Water Dynamics

The dynamics of water in the concentrated PNIPAM-d10 solution in $H_2O$ is investigated with QENS around $T_{cp}$. The polymer concentration of 26.7 wt % corresponds to a molar ratio of PNIPAM-d10 repeating units to water molecules of 1:19. This value is not much higher than the number of 11 water molecules that, on average, interact with each PNIPAM in the one-phase region,[57−61] i.e., most of the water is expected to be present in the form of hydration water.

The dynamic structure factors measured at $q$ = 1.65 $Å^{-1}$, i.e., at a $q$-value where coherent scattering from PNIPAM-d10 is insignificant (Figure S2 in the SI), are shown in Figure 4a together with the resolution function. The elastic line is rather weak. A quasi-elastic signal is observed that extends in energy beyond the elastic line. With increasing temperature, the inner part (within ca. ±0.3 meV) becomes narrower and is only slightly broader than the elastic line. Moreover, the quasi-elastic signal increases with temperature at larger energy transfers. A discontinuous change is observed at low energy

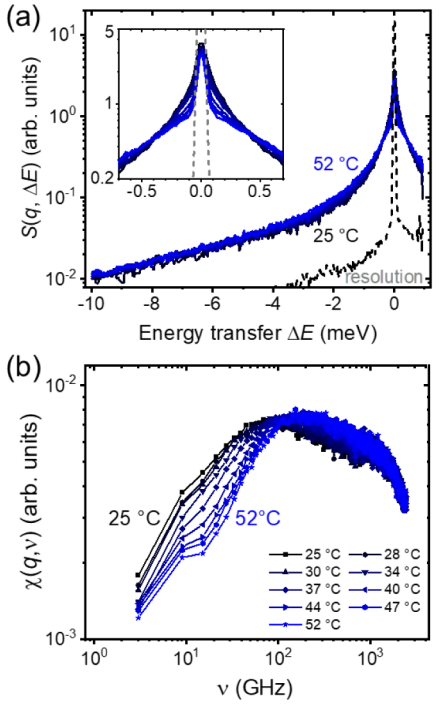


**Figure 4.** (a) Dynamic structure factors $S(q, \Delta E)$ of the PNIPAM-d10 solution in $H_2O$ at $q$ = 1.65 $Å^{-1}$ in dependence on temperature during a heating scan in semilogarithmic representation. From black to blue: 25, 28, 30, 34, 37, 40, 44, 47, and 52 °C. The gray dashed line is the elastic line from the measurement on vanadium. The inset shows the same data in the region close to the elastic line. (b) Corresponding imaginary part of the dynamic susceptibility $\chi(q, \nu)$ of the PNIPAM-d10 solution in $H_2O$ at $q$ = 1.65 $Å^{-1}$ in dependence on frequency in a double-logarithmic representation. Same colors as in (a); explanation of symbols, see legend.

transfers at temperatures between 37 and 40 °C (inset of Figure 4a).

To discriminate the contributions from bulk and hydration water, we transform the data into the imaginary part of the dynamic susceptibility, $\chi(q, \nu)$ (eq 1 and Figure 4b). In this representation, the weighting with the Bose factor (eq 2) reduces the elastic contribution, and the dynamic processes of hydration (typically in the frequency range below 100 GHz) and bulk water (typically above 100 GHz) are clearly discernible.[33,62,63]

The known maxima from the various relaxation processes of bulk water are observed at all temperatures above 100 GHz (Figure 4b). Their amplitudes increase with temperature. In addition, a relaxation peak is observed in $\chi(q, \nu)$ at low frequencies, indicating the presence of a large fraction of the hydration water. Its amplitude decreases with increasing temperature, suggesting that the chains dehydrate. Thus, a fraction of the hydration water is transformed into bulk water.

To evaluate the effect of the deuteration of PNIPAM on the dynamic susceptibilities, we plot selected curves of the PNIPAM-d10 solution together with the ones from a PNIPAM solution (data from ref 33) for representative temperatures below and above $T_{cp}$ (Figure 5). It is seen that for frequencies up to ca. 20 GHz, the amplitudes of $\chi(q, \nu)$ are lower in the PNIPAM-d10 solution than in the PNIPAM solution. The difference is rather weak below $T_{cp}$ (Figure 5a and b), while it is more significant above (Figure 5c and d). We note that the minimum frequencies that could be reached are different


https://doi.org/10.1021/acs.macromol.5c03241
Macromolecules 2026, 59, 4124−4133

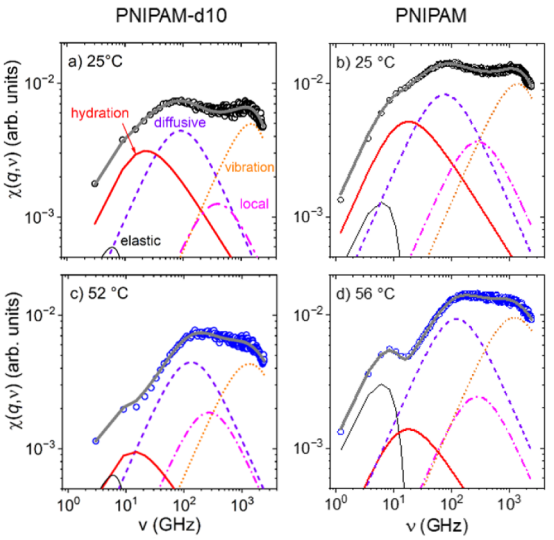


**Figure 5.** Imaginary part of the dynamic susceptibility $\chi(q, \nu)$ at $q$ = 1.65 Å$^{-1}$ of the PNIPAM-d10 (left) and of the PNIPAM solution in $H_2O$ (right) in dependence on frequency $\nu$ at the temperatures given in the graphs. Symbols: experimental data: full gray lines: overall fits. Deconvoluted contributions to the fitting function: elastic line (thin black full line), hydration water (red full line), diffusive process (violet dashed line), effective local process (magenta dash-dotted line), and vibrational process (orange dotted line).

(down to 3.0 GHz for PNIPAM-d10 and to 1.2 GHz for PNIPAM). The reduced frequency range in the data from the PNIPAM-d10 solution (in spite of the nominally higher energy resolution than for PNIPAM, ref 33) arises from difficulties in the background subtraction due to the low strength of the elastic line and the strongly anisotropic shape of the sample holder, resulting in strongly $q$-dependent shielding factors.

To quantify the fraction of hydration water and its dynamics, we fit the same model as described in ref 33:

$$\chi(q, \nu) = \chi_{el}(q, \nu) + \chi_h(q, \nu) + \chi_d(q, \nu) + \chi_l(q, \nu) + \chi_v(q, \nu) \quad (7)$$

where the elastic line is taken from the vanadium measurement (eq 6), the diffusional and the effective local processes of the bulk water fraction $\chi_d(q, \nu)$ and $\chi_l(q, \nu)$ are described by Debye functions (eq 3) and the vibrational process of the bulk water fraction $\chi_v(q, \nu)$ by a damped harmonic oscillator (DHO) function (eq 4). The relaxation of hydration water $\chi_h(q, \nu)$ is described by a Cole−Davidson function (eq 5). The deconvolutions are shown in Figure 5 for both solutions, and the fits are good in all cases. It is seen that the contribution from the hydration water strongly decreases upon heating through $T_{cp}$.

The fractions of hydration and bulk water are estimated by the ratio of amplitudes of the contributions as follows:

$$f_i = \frac{C_i(q)}{C_h(q) + C_d(q) + C_l(q)} \quad (8)$$

where $i$ = h, d, or l. The values from the measurements at $q$ = 1.65 Å$^{-1}$ are shown in Figure 6. The fraction of hydration water, $f_h$, decreases steadily from ca. 0.39 at 25 °C to 0.27 at 37 °C, then abruptly to 0.14 at 40 °C, and decreases further to 0.06 at 52 °C. The strong decrease of $f_h$ occurs between 37 and 40 °C, i.e., at a temperature slightly higher than $T_{cp}$ found

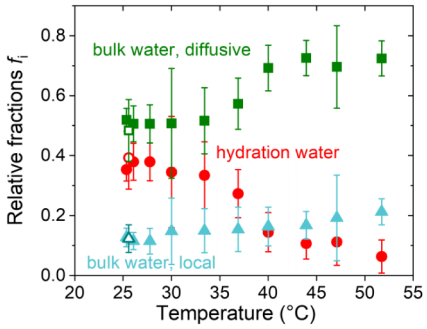


**Figure 6.** Results from QENS on a solution of the PNIPAM-d10 solution in $H_2O$. Fractions of hydration water, $f_h$ (red circles), and the diffusional and local processes of bulk water, $f_d$ (olive squares) and $f_l$ (cyan triangles), as a function of temperature from the measurements at $q$ = 1.65 Å$^{-1}$. The open symbols are from a measurement taken after cooling down.

using OM (36 ± 2 °C, Figure S1 in the SI). A similar mismatch between the value of $T_{cp}$ from turbidimetry and the temperature where changes are observed in the QENS data was observed previously[33] and may be due to a mismatch in the temperature calibration of the instruments. The fraction of the diffusive process of bulk water, $f_d$, increases abruptly between 37 and 40 °C, while the fraction of the local process of bulk water, $f_l$, increases slightly and steadily over the entire temperature range. Comparing with the values from the PNIPAM solution in $H_2O$,[33] it is found that the behavior of all three fractions is the same, with the exception of $f_h$, which continues to decrease in the PNIPAM-d10 solution up to the highest temperature, while it is constant in the PNIPAM solution.[33] The data points taken after cooling coincide with the ones from the heating run; i.e., the changes are reversible. The temperature dependencies of $f_h$ and $f_d$ are shown in Figure S3a in the SI.

The relaxation times of the hydration water, $\tau_h$, and of the diffusive and local processes, $\tau_d$ and $\tau_l$ of bulk water are shown at 28 °C, i.e., below $T_{cp}$, in dependence on the momentum transfer, $q$ (Figure 7). $\tau_h$ decreases with increasing $q$ from ca. 23 ps at 0.85 Å$^{-1}$ to ca. 6 ps at 1.85 Å$^{-1}$. These values are consistently lower than the ones from PNIPAM[33] and follow

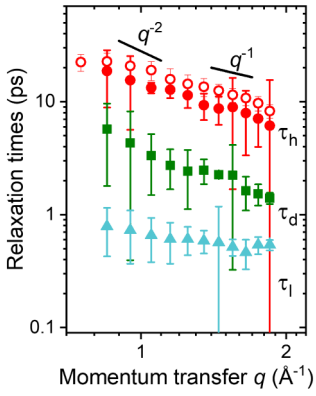


**Figure 7.** Relaxation time of hydration water, $\tau_h$ (closed red circles), and the diffusive and local processes of bulk water, $\tau_d$ (closed olive squares) and $\tau_l$ (closed cyan triangles) of the PNIPAM-d10 solution in $H_2O$, in dependence on momentum transfer $q$ at 28 °C. Open red circles: Values of $\tau_h$ for PNIPAM, taken from ref 33. The short lines indicate the dependences $\tau \propto q^{-2}$ and $\tau \propto q^{-1}$, respectively.


https://doi.org/10.1021/acs.macromol.5c03241
Macromolecules 2026, 59, 4124−4133

the same trend. Thus, the peak frequencies in the susceptibilities of PNIPAM are lower than those of PNIPAM-d10. We suspect that they were underestimated, probably due to the segmental dynamics of PNIPAM. Thus, suppressing the contribution of the PNIPAM dynamics by deuteration yields more accurate values. The $q$-dependence of $\tau_h$ is again consistent with isotropic jump diffusion, i.e., a $q^{-2}$ dependence at low $q$-values that becomes weaker at high $q$-values.[33] The temperature dependences of $\tau_h$ and $\tau_d$ at 1.65 Å$^{-1}$ are shown in Figure S4 in the SI.

To characterize the hydration water dynamics further, the range of energy transfers (and thus the frequencies) may be enlarged to lower values. At this time, we carried out high-resolution QENS experiments using a backscattering spectrometer. The dynamic structure factors at representative temperatures below and above $T_{cp}$ are shown in Figure S5a and b in the SI together with the resolution function. The elastic line is extremely weak, especially below $T_{cp}$, consistent with the fact that the polymer signal is largely suppressed by deuteration. Apart from the elastic line, a weak and broad process is observed. Transforming the dynamic structure factors into susceptibilities, using the same formalism as described above (eq 1), results in the data shown in Figure S5c. These follow the behavior $\chi(q, \nu) \propto \nu^1$, which is consistent with the shape of the Cole−Davidson function used to model the contribution of hydration water (eq 5, Figure 5). Shifting the values along the $\chi$-axis to match the magnitude of the signal from QENS shows that, at 29 °C, i.e., below $T_{cp}$, the hydration water contribution extends to much lower frequencies, down to ca. $10^{-1}$ GHz. This is also the case at 41 °C, i.e., above $T_{cp}$, and at this temperature, a weak signal of ultraslow water below 1 GHz seems to be present as well.

### 3.4. Polymer Segmental Dynamics

Temperature-resolved Raman spectra of the PNIPAM-d10 solution are displayed in Figure 8. They show multiple peaks due to the C−D vibrations, i.e., the hydrophobic hydration. Four main bands are present in the CD stretching region of PNIPAM-d10, namely near 2070 cm$^{-1}$, 2136 cm$^{-1}$, 2172 cm$^{-1}$, and 2240 cm$^{-1}$, which are assigned to symmetric stretching of the CD$_3$ groups in the side group ($\nu_s$(CD$_3$)), stretching of the CD groups ($\nu$(CD)), antisymmetric stretching of the CD$_2$ groups in the backbone ($\nu_{as}$(CD$_2$)) and antisymmetric stretching of the CD$_3$ side groups in the side group ($\nu_{as}$(CD$_3$)) (see Figure S6 in the SI). The peak frequencies of both the symmetric and the antisymmetric CD$_3$ stretching bands are nearly constant up to 37 °C and decrease above (Figure 9). The shifts occur near the temperature where

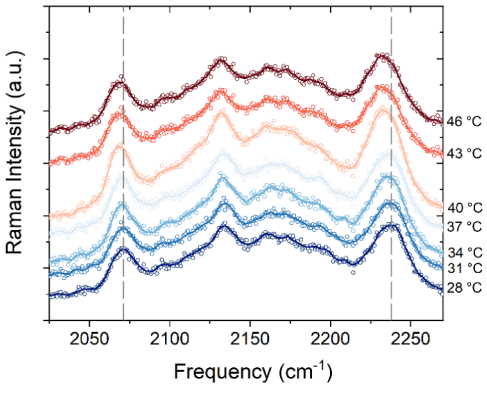


**Figure 8.** Raman spectra of the PNIPAM-d10 solution in $H_2O$ at the temperature given in the graph. For clarity, the curves were shifted vertically. Open symbols indicate raw data, and full lines represent the data smoothed with the Savitzky−Golay algorithm. Bluish colors indicate temperatures below $T_{cp}$ and reddish ones above. The analyzed vibrational bands correspond to the symmetric and antisymmetric stretching modes of CD$_3$, as indicated by the vertical dashed lines.

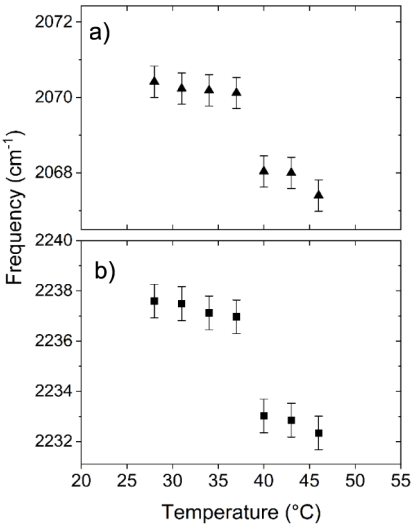


**Figure 9.** Peak frequencies of (a) the symmetric and (b) the antisymmetric CD$_3$ stretching bands, $\nu_s$(CD$_3$) and $\nu_{as}$(CD$_3$), of the PNIPAM-d10 solution in $H_2O$, in dependence on temperature. Error bars indicate uncertainties obtained from the spectral fits.

changes were observed in the QENS results; hence, we attribute this temperature to $T_{cp}$. The Raman results point to a change in hydration between the CD$_3$ groups in the isopropyl side group of PNIPAM-d10 and $H_2O$ as the two-phase state is entered. In comparison, protiated PNIPAM exhibits analogous behavior in the CH-stretching region, where the frequencies of the symmetric and antisymmetric CH$_3$ bands decrease sharply above $T_{cp}$, reflecting similar changes in hydrophobic hydration.

## 4. CONCLUSIONS

A perdeuterated PNIPAM-d10 sample was synthesized by radical polymerization, and the deuteration was verified by $^2$H NMR, FT-IR, and Raman spectroscopy. The demixing temperature, as determined using optical microscopy, is notably, i.e., by a few degrees centigrade, higher than that of a protiated PNIPAM homopolymer of virtually the same molar mass and dispersity at the same polymer concentration.[33] Using QENS, it is found that the elastic line is indeed significantly weakened compared to the one of PNIPAM in $H_2O$.[33] Thus, the contribution of the segmental dynamics of the polymer is suppressed, as expected, and its overlap with the signal from the hydration water is reduced. Conversion of the dynamic structure factors into dynamic susceptibilities revealed that the signal of the hydration water is present and shows the same characteristics as those in PNIPAM: the fraction of hydration water decreases abruptly near $T_{cp}$, and the $q$-dependence of its relaxation time follows that expected for jump diffusion. However, the peak relaxation times of the hydration water of PNIPAM-d10 are lower than the ones observed in protiated PNIPAM.[33] High-resolution QENS


https://doi.org/10.1021/acs.macromol.5c03241
Macromolecules 2026, 59, 4124−4133

reveals that the slow process in the dynamic susceptibility follows the frequency behavior expected for the hydration water down to ca. $1 \times 10^{-1}$ GHz.

While QENS probes the incoherent motion of the hydration water, Raman spectroscopy provides a site-specific probe of the alkyl groups. At the LCST transition, there is a steep frequency shift of the C−D stretching vibrations of the perdeuterated side groups. The onset temperature is in good agreement with that determined macroscopically by optical microscopy. The abrupt shifts of the C−D stretching vibrations are analogous to the discontinuous change previously reported for the C−H stretching vibrations in PNIPAM. These observations support the assignment of the frequency shifts to changes in the degree of hydration of the side groups, linking the spectroscopic signatures directly to the temperature-induced phase transition. The QENS and Raman results provide a consistent picture in which the abrupt spectroscopic changes originate from dehydration of the side groups, reflecting the distinct roles of local hydration and polymer conformation in driving the phase transition. They provide sensitive tests for molecular dynamics computations.

## ■ ASSOCIATED CONTENT

### Supporting Information

The Supporting Information is available free of charge at https://pubs.acs.org/doi/10.1021/acs.macromol.5c03241.

Cloud point determination by optical imaging; neutron diffraction measurements with polarization analysis; additional results from quasi-elastic neutron scattering; high-resolution quasi-elastic neutron scattering; and deconvolution of Raman spectra (PDF)

## ■ AUTHOR INFORMATION


### Corresponding Authors

**Christine M. Papadakis** − *Technical University of Munich, TUM School of Natural Sciences, Department of Physics, Soft Matter Physics Group, Garching 85748, Germany;* orcid.org/0000-0002-7098-3458; Email: papadakis@tum.de

**Alfons Schulte** − *Department of Physics and College of Optics and Photonics, University of Central Florida, Orlando, Florida 32816-2385, United States;* orcid.org/0000-0003-0824-8572; Email: Alfons.schulte@ucf.edu

### Authors

**Eric Rende** − *Department of Physics and College of Optics and Photonics, University of Central Florida, Orlando, Florida 32816-2385, United States*

**Feifei Zheng** − *Technical University of Munich, TUM School of Natural Sciences, Department of Physics, Soft Matter Physics Group, Garching 85748, Germany;* orcid.org/0000-0002-1070-2829

**Bahar Yazdanshenas** − *Technical University of Munich, TUM School of Natural Sciences, Department of Physics, Soft Matter Physics Group, Garching 85748, Germany*

**Marcell Wolf** − *Heinz Maier-Leibnitz Zentrum (MLZ), Technische Universität München, Garching 85748, Germany*

**Michaela Zamponi** − *Forschungszentrum Jülich GmbH, Jülich Centre for Neutron Science (JCNS) at Heinz Maier-Leibnitz Zentrum (MLZ), Garching 85748, Germany;* orcid.org/0009-0007-2735-588X

[▽]**Marie-Sousai Appavou** − *Forschungszentrum Jülich GmbH, Jülich Centre for Neutron Science (JCNS) at Heinz Maier-Leibnitz Zentrum (MLZ), Garching 85748, Germany*

**Thomas Müller** − *Forschungszentrum Jülich GmbH, Jülich Centre for Neutron Science (JCNS) at Heinz Maier-Leibnitz Zentrum (MLZ), Garching 85748, Germany*

**Dharani Mullapudi** − *Department of Physics and College of Optics and Photonics, University of Central Florida, Orlando, Florida 32816-2385, United States*

**Alec Nieth** − *Department of Physics and College of Optics and Photonics, University of Central Florida, Orlando, Florida 32816-2385, United States*

**Dirk Schanzenbach** − *Universität Potsdam, Institut für Chemie, Potsdam 14476, Germany*

**André Laschewsky** − *Universität Potsdam, Institut für Chemie, Potsdam 14476, Germany; Fraunhofer-Institut für Angewandte Polymerforschung, Potsdam 14476, Germany;* orcid.org/0000-0003-2443-886X

Complete contact information is available at: https://pubs.acs.org/10.1021/acs.macromol.5c03241


### Author Contributions

The manuscript was written through contributions of all authors. All authors have given their approval to the final version of the manuscript.


### Funding

Deutsche Forschungsgemeinschaft is acknowledged for funding (Deutsche Forschungsgemeinschaft) (PA 771/22−1). A. S. acknowledges support by an August-Wilhelm Scheer visiting professorship at TU Munich.


### Notes

The authors declare no competing financial interest.
[▽]M.-S.A. Deceased.


## ■ ACKNOWLEDGMENTS

We thank Dr. Jia-Jhen Kang (Technical University of Munich) and Dr. Bart-Jan Niebuur (INM − Leibniz Institute for New Materials, Saarbrücken, Germany) for their help with the experiment and for the fruitful discussions. We also thank Dr. Wiebke Lohstroh and Herbert Meier for designing the sample cell. This work is based on experiments performed at the DNS and SPHERES instruments operated by Forschungszentrum Jülich, and the TOFTOF instrument operated by the Technical University of Munich at the Heinz Maier-Leibnitz Zentrum (MLZ), Garching, Germany. We thank them for excellent equipment.


## ■ REFERENCES


(1) Bellissent-Funel, M.-C.; Hassanali, A.; Havenith, M.; Henchman, R.; Pohl, P. S.; Sterpone, F.; van der Spoel, D.; Xu, Y.; Garcia, A. Water Determines the Structure and Dynamics of Proteins. *Chem. Rev.* **2016**, *116*, 7673−7697.

(2) Laage, D.; Elsaesser, T.; Hynes, J. T. Water Dynamics in the Hydration Shells of Biomolecules. *Chem. Rev.* **2017**, *117*, 10694−10725.

(3) Kauzmann, W. Some Factors in The Interpretation of Protein Denaturation. *Adv. Protein Chem.* **1959**, *14*, 1−63.

(4) Baldwin, R. L. Dynamic Hydration Shell Restores Kauzmann's 1959 Explanation of How the Hydrophobic Factor Drives Protein Folding. *Proc. Natl. Acad. Sci. U. S. A.* **2014**, *111*, 13052−13056.

(5) Tavagnacco, L.; Del Galdo, S.; Galli, A.; Capone, B.; Zaccarelli, E.; Chiessi, E. Understanding The Lower Critical Solution Temper-

ature of Amphiphilic Synthetic Polymers in Water: The Role of Conformation and Hydration. *J. Mol. Liq.* **2025**, *429*, 127646.
(6) Aseyev, V.; Tenhu, H.; Winnik, F. M. Non-ionic Thermoresponsive Polymers in Water. *Adv. Polym. Sci.* **2010**, *242*, 29−89.
(7) Mukherji, D.; Marques, C. M.; Kremer, K. Smart Responsive Polymers: Fundamentals and Design Principles. *Annu. Rev. Condens. Matter Phys.* **2020**, *11*, 271−299.
(8) Maeda, Y.; Nakamura, T.; Ikeda, I. Changes in the Hydration States of Poly(*N*-*n*-propylmethacrylamide) and Poly(*N*-isopropylmethacrylamide) during Their Phase Transitions in Water Observed by FTIR Spectroscopy. *Macromolecules* **2001**, *34*, 8246−8251.
(9) Ohta, H.; Ando, I.; Fujishige, S.; Kubota, K. Molecular Motion and $^1$H NMR Relaxation of Aqueous Poly(*N*-isopropylacrylamide) Solution Under High Pressure. *J Polym Sci B Polym Phys.* **1991**, *29*, 963−968.
(10) Starovoytova, L.; Spěváček, J. Effect of Time on the Hydration and Temperature-Induced Phase Separation in Aqueous Polymer Solutions. $^1$H NMR Study. *Polymer* **2006**, *47*, 7329−7334.
(11) Kametani, S.; Sekine, S.; Ohkubo, T.; Hirano, T.; Ute, K.; Cheng, H. N.; Asakura, T. NMR Studies of Water Dynamics During Sol-to-gel Transition of Poly(*N*-isopropylacrylamide) in Concentrated Solution. *Polymer* **2017**, *109*, 287−296.
(12) Buratti, E.; Tavagnacco, L.; Zanatta, M.; Chiessi, E.; Buoso, S.; Franco, S.; Ruzicka, B.; Angelini, R.; Orecchini, A.; Bertoldo, M.; Zaccarelli, E. The Role of Polymer Structure on Water Confinement in Poly(*N*-isopropylacrylamide) Dispersions. *J. Mol. Liq.* **2022**, *355*, 118924.
(13) Ceriotti, M.; Fang, W.; Kusalik, P. G.; McKenzie, R. H.; Michaelides, A.; Morales, M. A.; Markland, T. A. Nucelar Quantum Effects in Water and Aqueous Systems: Experiment, Theory, and Current Challenges. *Chem. Rev.* **2016**, *116*, 7529−7550.
(14) Turowski, M.; Yamakawa, N.; Meller, J.; Kimata, K.; Ikegami, T.; Hosoya, K.; Tanaka, N.; Thornton, E. R. Deuterium Isotope Effects on Hydrophobic Interactions: The Importance of Dispersion Interactions in the Hydrophobic Phase. *J. Am. Chem. Soc.* **2003**, *125*, 13836−13849.
(15) Malik, R.; Stolte, N.; Forbert, H.; Chandra, A.; Marx, D. Accurate Determination of Isotope Effects on the Dynamics of H-Bond Breaking and Making in Liquid Water. *J. Phys. Chem. Lett.* **2025**, *16*, 3727−3733.
(16) Higgins, J. S. Neutron Scattering from Polymers: Five Decades of Developing Possibilities. *Annu. Rev. Chem. Biomol. Eng.* **2016**, *7*, 1−28.
(17) Almdal, K.; Rosedale, J. H.; Bates, F. S.; Wignall, G. D.; Fredrickson, G. H. Gaussian- to Stretched-Coil Transition in Block Copolymer Melts. *Phys. Rev. Lett.* **1990**, *65*, 1112−1115.
(18) Hadziioannou, G.; Picot, C.; Skoukios, A.; Ionescu, M.-L.; Mathis, A.; Duplessix, R.; Gallot, Y.; Lingelser, J. P. Low-angle Neutron Scattering Study of the Lateral Extension of Chains in Lamellar Styrene Isoprene Block Copolymers. *Macromolecules* **1982**, *15*, 263−267.
(19) Gerstl, C.; Brodeck, M.; Schneider, G. J.; Su, Y.; Allgaier, J.; Arbe, A.; Colmenero, J.; Richter, D. Short and Intermediate Range Order in Poly(alkylene oxide)s. A Neutron Diffraction and Molecular Dynamics Simulation Study. *Macromolecules* **2012**, *45*, 7293−7303.
(20) Halperin, A.; Kröger, M.; Winnik, F. M. Poly(*N*-isopropylacrylamide) Phase Diagrams: Fifty Years of Research. *Angew. Chem., Int. Ed.* **2015**, *54*, 15342−15367.
(21) Kujawa, P.; Winnik, F. M. Volumetric Studies of Aqueous Polymer Solutions Using Pressure Perturbation Calorimetry: A New Look at the Temperature-Induced Phase Transition of Poly(*N*-isopropylacrylamide) in Water and $D_2O$. *Macromolecules* **2001**, *34*, 4130−4135.
(22) Gorelov, A. V.; Du Chesne, A.; Dawson, K. A. Phase Separation in Dilute Solutions of Poly(*N*-isopropylacrylamide). *Physica A* **1997**, *240*, 443−452.
(23) Chan, K.; Pelton, R.; Zhang, J. On the Formation of Colloidally Dispersed Phase Separated Poly(*N*-isopropylacrylamide). *Langmuir* **1999**, *15*, 4018−4020.
(24) Chuang, J.; Grosberg, A. Y.; Tanaka, T. Topological Repulsion between Polymer Globules. *J. Chem. Phys.* **2000**, *112*, 6434−6442.
(25) Wu, C.; Li, W.; Zhu, X. X. Viscoelastic Effect on the Formation of Mesoglobular Phase in Dilute Solutions. *Macromolecules* **2004**, *37*, 4989−4992.
(26) Aseyev, V.; Hietala, S.; Laukkanen, A.; Nuopponen, M.; Confortini, O.; Du Prez, F. E.; Tenhu, H. Mesoglobules of Thermoresponsive Polymers in Dilute Aqueous Solutions Above the LCST. *Polymer* **2005**, *46*, 7118−7131.
(27) Kujawa, P.; Aseyev, V.; Tenhu, H.; Winnik, F. M. Temperature-sensitive Properties of Poly(*N*-isopropylacrylamide) Mesoglobules Formed in Dilute Aqueous Solutions Heated Above Their Demixing Point. *Macromolecules* **2006**, *39*, 7686−7693.
(28) Balu, C.; Delsanti, M.; Guenoun, P.; Monti, F.; Cloitre, M. Colloidal Phase Separation of Concentrated PNIPAm Solutions. *Langmuir* **2007**, *23*, 2404−2407.
(29) Niebuur, B.-J.; Claude, K.-L.; Pinzek, S.; Cariker, C.; Raftopoulos, K. N.; Pipich, V.; Appavou, M.-S.; Schulte, A.; Papadakis, C. M. Pressure-dependence of Poly(*N*-isopropylacrylamide) Mesoglobule Formation in Aqueous Solution. *ACS Macro Lett.* **2017**, *6*, 1180−1185.
(30) Tavagnacco, L.; Chiessi, E.; Zaccarelli, E. Molecular Insights on Poly(*N*-isopropylacrylamide) Coil-to-globule Transition Induced by Pressure. *Phys. Chem. Chem. Phys.* **2021**, *23*, 5984−5991.
(31) Telling, M. T. F. *A Practical Guide to Quasi-elastic Neutron Scattering*; Royal Society of Chemistry, 2020. .
(32) Philipp, M.; Kyriakos, K.; Silvi, L.; Lohstroh, W.; Petry, W.; Krüger, J. K.; Papadakis, C. M.; Müller-Buschbaum, P. From Molecular Dehydration to Excess Volumes of Phase-separating PNIPAM Solutions. *J. Phys. Chem. B* **2014**, *118*, 4253−4260.
(33) Niebuur, B.-J.; Lohstroh, W.; Appavou, M.-S.; Schulte, A.; Papadakis, C. M. Water Dynamics in a Concentrated Poly(*N*-isopropylacrylamide) Solution at Variable Pressure. *Macromolecules* **2019**, *52*, 1942−1954.
(34) Wang, W.; Metwalli, E.; Perlich, J.; Papadakis, C. M.; Cubitt, R.; Müller-Buschbaum, P. Cyclic Switching of Water Storage in Thin Block Copolymer Films Containing Poly(*N*-isopropylacrylamide). *Macromolecules* **2009**, *42*, 9041−9051.
(35) Cors, M.; Wiehemeier, L.; Oberdisse, J.; Hellweg, T. Deuteration-Induced Volume Phase Transition Temperature Shift of PNIPMAM Microgels. *Polymers* **2019**, *11*, 620.
(36) Mohanty, P. S.; Nöjd, S.; van Gruijthuijsen, K.; Crassous, J. J.; Obiols-Rabasa, M.; Schweins, R.; Stradner, A.; Schurtenberger, P. Interpenetration of Polymeric Microgels at Ultrahigh Densities. *Sci. Rep.* **2017**, *7*, 1487.
(37) Brugnoni, M.; Nickel, A. C.; Kröger, L. C.; Scotti, A.; Pich, A.; Leonhard, K.; Richtering, W. Synthesis and Structure of Deuterated Ultra-low Cross-linked Poly(*N*-isopropylacrylamide) Microgels. *Polym. Chem.* **2019**, *10*, 2397−2405.
(38) Nevolianis, T.; Scotti, A.; Petrunin, A. V.; Richtering, W.; Leonhard, K. Understanding the Monomer Deuteration Effect on the Transition Temperature of Poly(*N*-isopropylacrylamide) Microgels in $H_2O$. *Polym. Chem.* **2023**, *14*, 1447−1455.
(39) Sbeih, S.; Mohanty, P. S.; Morrow, M. R.; Yethiraj, A. Structural Parameters of Soft PNIPAM Microgel Particles as a Function of Crosslink Density. *J. Colloid Interface Sci.* **2019**, *552*, 781−793.
(40) Su, Y.; Nemkovski, K.; Demirdis, S. DNS: Diffuse Scattering Neutron Time-of-flight Spectrometer. *JLSRF* **2015**, *1*, A27.
(41) Unruh, T.; Neuhaus, J.; Petry, W. The High resolution Time-of-flight Spectrometer TOFTOF. *Nucl. Instrum. Methods Phys. Res., Sect. A* **2007**, *580*, 1414−1422.
(42) Lohstroh, W.; Evenson, Z. TOFTOF: Cold Neutron Time-of-flight Spectrometer. *JLSRF* **2015**, *1*, A15.
(43) Appavou, M.-S.; Busch, S.; Doster, W.; Gaspar, A.; Unruh, T. The Influence of 2 kbar Pressure on the Global and Internal Dynamics of Human Hemoglobin Observed by Quasielastic Neutron Scattering. *Eur. Biophys. J.* **2011**, *40*, 705−714.


https://doi.org/10.1021/acs.macromol.5c03241
*Macromolecules* 2026, 59, 4124−4133

(44) Paalman, H. H.; Pings, C. J. Numerical Evaluation of X-ray Absorption Factors for Cylindrical Samples and Annular Sample Cells. *J. Appl. Phys.* **1962**, *33*, 2635−2639.
(45) Zeidler, A. X-ray and Neutron Attenuation Correction Factors for Spherical Samples. *J. Appl. Crystallogr.* **2012**, *45*, 122−123.
(46) Arnold, O.; et al. Mantid-Data Analysis and Visualization Package for Neutron Scattering and $\mu$ SR Experiments. *Nucl. Instrum. Methods Phys. Res., Sect. A* **2014**, *764*, 156−166.
(47) Doster, W.; Cusack, S.; Petry, W. Dynamical Instability of Liquidlike Motions in a Globular Protein Observed by Inelastic Neutron Scattering. *Phys. Rev. Lett.* **1990**, *65*, 1080−1083.
(48) Arbe, A.; Malo de Molina, P.; Alvarez, F.; Frick, B.; Colmenero, J. Dielectric Susceptibility of Liquid Water: Microscopic Insights from Coherent and Incoherent Neutron Scattering. *Phys. Rev. Lett.* **2016**, *117*, 185501.
(49) Wuttke, J.; Budwig, A.; Drochner, M.; Kämmerling, H.; Kayser, F.-J.; Kleines, H.; Ossovyi, V.; Pardo, L. C.; Prager, M.; Richter, D.; Schneider, G. J.; Schneider, H.; Staringer, S. S. Jülich's High-flux Neutron Backscattering Spectrometer at FRM II. *Rev. Sci. Instrum.* **2012**, *83*, 075109.
(50) Zamponi, M.; Khaneft, M. SPHERES: Backscattering Spectrometer. *JLSRF* **2015**, *1*, A30.
(51) Bivigou-Koumba, A. M.; Kristen, J.; Laschewsky, A.; Müller-Buschbaum, P.; Papadakis, C. M. Synthesis of Symmetrical Triblock Copolymers of Styrene and *N*-isopropylacrylamide Using Bifunctional Bis(trithiocarbonate)s as RAFT Agents. *Macromol. Chem. Phys.* **2009**, *210*, 565−578.
(52) Ko, C.-H.; Henschel, C.; Meledam, G. P.; Schroer, M. A.; Müller-Buschbaum, P.; Laschewsky, A.; Papadakis, C. M. Self-Assembled Micelles from Thermoresponsive Poly(methyl methacrylate)-*b*-poly(*N*-isopropylacrylamide) Diblock Copolymers in Aqueous Solution. *Macromolecules* **2021**, *54*, 384−397.
(53) Sun, B.; Lin, Y.; Wu, P. Structure Analysis of Poly(*N*-isopropylacrylamide) Using Near-infrared Spectroscopy and Generalized Twodimensional Correlation Infrared Spectroscopy. *Appl. Spectrosc.* **2007**, *61*, 765−771.
(54) Bucatariu, S.; Fundueanu, G.; Prisacaru, I.; Balan, M.; Stoica, I.; Harabagiu, V.; Constantin, M. Synthesis and Characterization of Thermosensitive Poly(*N*-isopropylacrylamide-co-hydroxyethylacrylamide) Microgels as Potential Carriers for Drug Delivery. *J. Polym. Res.* **2014**, *21*, 580.
(55) Futscher, M. H.; Philipp, M.; Müller-Buschbaum, P.; Schulte, A. The Role of Backbone Hydration of Poly(*N*-isopropyl acrylamide) Across the Volume Phase Transition Compared to its Monomer. *Sci. Rep.* **2017**, *7*, 17012.
(56) Schulte, A.; Harms, N.; Rende, E.; Mullapudi, D.; Nieth, A.; Bennett, C.; Schanzenbach, D.; Laschewsky, A.; Papadakis, C. M. Vibrational Spectroscopy of Perdeuterated Poly(*N*-isopropylacrylamide) Solutions and Hydration Changes Across the Demixing-Transition. In *87th Annual Conference of the DPG and DPG Spring Meeting*; DPG: Berlin, 2024.
(57) Shibayama, M.; Morimoto, M.; Nomura, M. Phase Separation Induced Mechanical Transition of Poly(*N*-isopropylacrylamide)/Water Isochore Gels. *Macromolecules* **1994**, *27*, 5060−5066.
(58) Ono, Y.; Shikata, T. Contrary Hydration Behavior of *N*-Isopropylacrylamide to its Polymer, P(NIPAm), with a Lower Critical Solution Temperature. *J. Phys. Chem. B* **2007**, *111*, 1511−1513.
(59) Deshmukh, S. A.; Sankaranarayanan, S. K. R. S.; Suthar, K.; Mancini, D. C. Role of Solvation Dynamics and Local Ordering of Water in Inducing Conformational Transitions in Poly(*N*-isopropylacrylamide) Oligomers through the LCST. *J. Phys. Chem. B* **2012**, *116*, 2651−2663.
(60) Füllbrandt, M.; Ermilova, E.; Asadujjaman, A.; Hölzel, R.; Bier, F.; von Klitzing, R.; Schönhals, A. Dynamics of Linear Poly(*N*-isopropylacrylamide) in Water around the Phase Transition Investigated by Dielectric Relaxation Spectroscopy. *J. Phys. Chem. B* **2014**, *118*, 3750−3759.
(61) Shiraga, K.; Naito, H.; Suzuki, T.; Kondo, N.; Ogawa, Y. Hydration and Hydrogen Bond Network of Water during the Coil-to-Globule Transition in Poly(*N*isopropylacrylamide) Aqueous Solution at Cloud Point Temperature. *J. Phys. Chem. B* **2015**, *119*, 5576−5587.
(62) Settles, M.; Doster, W. Anomalous Diffusion of Adsorbed Water: A Neutron Scattering Study of Hydrated Myoglobin. *Faraday Discuss.* **1996**, *103*, 269−279.
(63) Malo de Molina, P.; Alvarez, F.; Frick, B.; Wildes, A.; Arbe, A.; Colmenero, J. Investigation of the Dynamics of Aqueous Proline Solutions Using Neutron Scattering and Molecular Dynamics Simulations. *Phys. Chem. Chem. Phys.* **2017**, *19*, 27739−27754.




https://doi.org/10.1021/acs.macromol.5c03241
*Macromolecules* 2026, 59, 4124−4133